frontiers | Frontiers in Neuroscience

TYPE Original Research
PUBLISHED 25 May 2023
DOI 10.3389/fnins.2023.1177044

OPEN ACCESS

EDITED BY
Nico Sollmann,
University of California, San Francisco,
United States

REVIEWED BY
Yang Yingjian,
Northeastern University, China
Chaoran Yang,
Northeastern University, China

*CORRESPONDENCE
Yuehua Li
✉ liyuehua312@163.com

†These authors have contributed equally to this work

RECEIVED 01 March 2023
ACCEPTED 02 May 2023
PUBLISHED 25 May 2023

CITATION
He R, Zhou J, Xu X, Wei X, Wang F and Li Y (2023) Comparing the predictive value of quantitative magnetic resonance imaging parametric response mapping and conventional perfusion magnetic resonance imaging for clinical outcomes in patients with chronic ischemic stroke.
Front. Neurosci. 17:1177044.
doi: 10.3389/fnins.2023.1177044

Comparing the predictive value of quantitative magnetic resonance imaging parametric response mapping and conventional perfusion magnetic resonance imaging for clinical outcomes in patients with chronic ischemic stroke

Rui He[1†], Jia Zhou[1†], Xiaoyu Xu[1], Xiaoer Wei[1], Feng Wang[2] and Yuehua Li[1*]

[1]Department of Radiology, Shanghai Sixth People's Hospital Affiliated to Shanghai Jiao Tong University School of Medicine, Shanghai, China, [2]Department of Neurology, Shanghai Sixth People's Hospital Affiliated to Shanghai Jiao Tong University School of Medicine, Shanghai, China

Predicting clinical outcomes after stroke, using magnetic resonance imaging (MRI) measures, remains a challenge. The purpose of this study was to investigate the prediction of long-term clinical outcomes after ischemic stroke using parametric response mapping (PRM) based on perfusion MRI data. Multiparametric perfusion MRI datasets from 30 patients with chronic ischemic stroke were acquired at four-time points ranging from V2 (6 weeks) to V5 (7 months) after stroke onset. All perfusion MR parameters were analyzed using the classic whole-lesion approach and voxel-based PRM at each time point. The imaging biomarkers from each acquired MRI metric that was predictive of both neurological and functional outcomes were prospectively investigated. For predicting clinical outcomes at V5, it was identified that PRM_{Tmax-}, PRM_{rCBV-}, and PRM_{rCBV+} at V3 were superior to the mean values of the corresponding maps at V3. We identified correlations between the clinical prognosis after stroke and MRI parameters, emphasizing the superiority of the PRM over the whole-lesion approach for predicting long-term clinical outcomes. This indicates that complementary information for the predictive assessment of clinical outcomes can be obtained using PRM analysis. Moreover, new insights into the heterogeneity of stroke lesions revealed by PRM can help optimize the accurate stratification of patients with stroke and guide rehabilitation.

KEYWORDS

ischemic stroke, parametric response mapping, perfusion MRI, prediction, prognosis

Introduction

Ischemic stroke, caused by impaired blood flow to the brain, is a major cause of death and long-term disability globally (Sennfält et al., 2021; Whiteley and Gupta, 2021). The evaluation of clinical outcomes is important for predicting the likelihood of survival and quality of life in patients after a stroke. Clinical outcomes are generally rated using the National Institutes of Health Stroke Scale (NIHSS) or the modified Rankin Scale (mRS) due to their validity and availability to discriminate clinically relevant grades of individual status after ischemic stroke (Banks and Marotta, 2007; König et al., 2008; Liu X. et al., 2022; Liu Y. et al., 2022). A non-invasive neuroimaging technique is essential for stroke assessment. Both computed tomography (CT) and magnetic resonance imaging (MRI) protocols provide excellent tools for the evaluation of cerebral tissue injury, vessel status, and cerebral perfusion. MRI has better accuracy for the identification of the intraluminal thrombus, previous chronic lobar ischemia, and hemorrhagic transformation and does not involve the use of ionizing radiation (Audebert and Fiebach, 2015; Vilela and Rowley, 2017). Perfusion-weighted imaging (PWI), one sequence of MRI, can delineate regions of abnormal perfusion that reflect the degree of functional impairment and structural damage (Włodarczyk and Cichon, 2022).

Considering the usefulness and accessibility of MRI, accurate and early clinical outcome prediction using MRI biomarkers is achievable. Clinically predicting post-stroke clinical outcomes using conventional MRI measurements remains a challenge. Generally, MRI parameters are based on pre-defined regions of interest (ROIs) that are manually or automatically delineated; these are based on pixels with values that differ significantly between lesion areas and healthy tissue. On a parametric map, the intralesional characteristics are shown using the mean values of the pixels in the ROI. However, analyzing mean voxel values in ROIs can easily mask focal changes in intralesional tissue properties and hide details that reflect stroke development. Parametric response mapping (PRM) analyzes parametric values voxel by voxel using co-registered longitudinal MRI maps. It has been proven to be distinctly advantageous over whole-lesion analysis techniques using mean values and histograms of all the pixels in ROIs in studies on tumors and chronic obstructive pulmonary disease (Hamstra et al., 2008; Tsien et al., 2010; Galbán et al., 2012) and has been translated to cerebrovascular disease (Tsai et al., 2013; He et al., 2017). PRM also allows for the classification of individual ROI-contained voxels based on the extent of changes in values that are spatially dependent. To date, it has been applied using a wide variety of diffusion- and perfusion-based quantitative MRI parameters (Moffat et al., 2005; Galbán et al., 2009; Cho et al., 2014; Baer et al., 2015).

Compared to acute stroke, the understanding of cerebral perfusion in chronic stroke is far less clear (Richardson et al., 2011). In the present study, we compared the ability of PRM and a whole-lesion approach using ROIs to identify the development of ischemic tissue in patients with chronic clinical stroke. Accordingly, we examined the linear correlation between imaging parameters (mean values and PRM-derived measurements) and clinical outcomes as assessed using the NIHSS and the mRS. We hypothesized that PRM could reveal more details on the relationship between perfusion-weighted imaging parameters and long-term clinical outcomes. Furthermore, we predicted that using conventional MRI parameters with PRM analysis would be a better predictor of long-term clinical outcomes than the classic whole-lesion approach.

Materials and methods

Patient population

From January 2017 to January 2018, 98 patients with chronic stroke examined and treated by standard physical and occupational therapy in the Department of Neurology were consecutively evaluated after the confirmation of diagnosis using clinical evidence, including stroke-related symptoms and initial positive findings on diffusion-weighted imaging (DWI). The study inclusion criteria were (1) right or left ischemic stroke within the internal carotid artery territory; (2) neurological deficits persisting for 7 days after stroke onset (NIHSS = 9–23); and (3) patients who did not receive intravenous thrombolysis or mechanical thrombectomy therapy. The exclusion criteria included (1) the absence of clinical or imaging data; (2) a history of neurological or psychiatric disorder; (3) posterior circulation stroke; (4) severe MRI artifacts; and (5) intravenous thrombolysis or intravascular treatment before MRI scans. In addition, patients with substance abuse, claustrophobia, a major decline in consciousness, or hemorrhagic transformation were not included in this study. Patients who withdrew their consent to participate were also excluded. Finally, a total of 30 patients (21 men, 9 women; mean age 51.5 ± 10.3 years, range 42–67 years) were enrolled in the study (Figure 1). A total of 30 healthy control participants underwent clinical and MRI assessments at baseline. The protocol for this study was approved by the local institutional review board.

For the design of the clinical protocol, five post-stroke time points (V1: 7 days; V2: 6 weeks, V3: 3 months, V4: 5 months, and V5: 7 months) were chosen to monitor the progression of the disease after stroke onset. All 30 patients underwent MRI scans at four time points (V2–V5). NIHSS and mRS assessments were performed at each time point (V1–V5). NIHSS and mRS scores obtained at V2–V5 were used to analyze correlations between imaging metrics and clinical outcome scores. The rates of change in the NIHSS and mRS scores between each pair of continuous time points were also measured.

To verify the efficiency of functional outcome prediction using different approaches, all 30 patients were stratified into good- or poor-outcome subgroups according to their individual final functional outcome (V5 mRS scores). In the good-outcome subgroup ($n = 8$), the mRS scores estimated at V5 ranged from 0 to 2, and these scores for the poor-outcome subgroup ranged from 3 to 6 ($n = 22$), based on previous research (Tsai et al., 2013; Hendrix et al., 2022).

Imaging acquisition

Imaging was carried out on a 3.0-T Achieva MRI scanner (Philips, Amsterdam, Netherlands), using a whole-body radiofrequency transmitter and 8-channel head receiver coils. Conventional scanning sequences, routinely performed in our clinic, included 3D gradient-recalled echo T1-weighted imaging (matrix: 512 × 512, repetition time [TR]/echo time [TE]: 9.8/4.6 ms, thickness: 1 mm, gap: 1 mm), T2-weighted imaging (matrix: 512 × 512, TR/TE: 8500/80 ms, thickness: 4 mm, gap: 1 mm), and T2 fluid-attenuated inversion recovery (T2

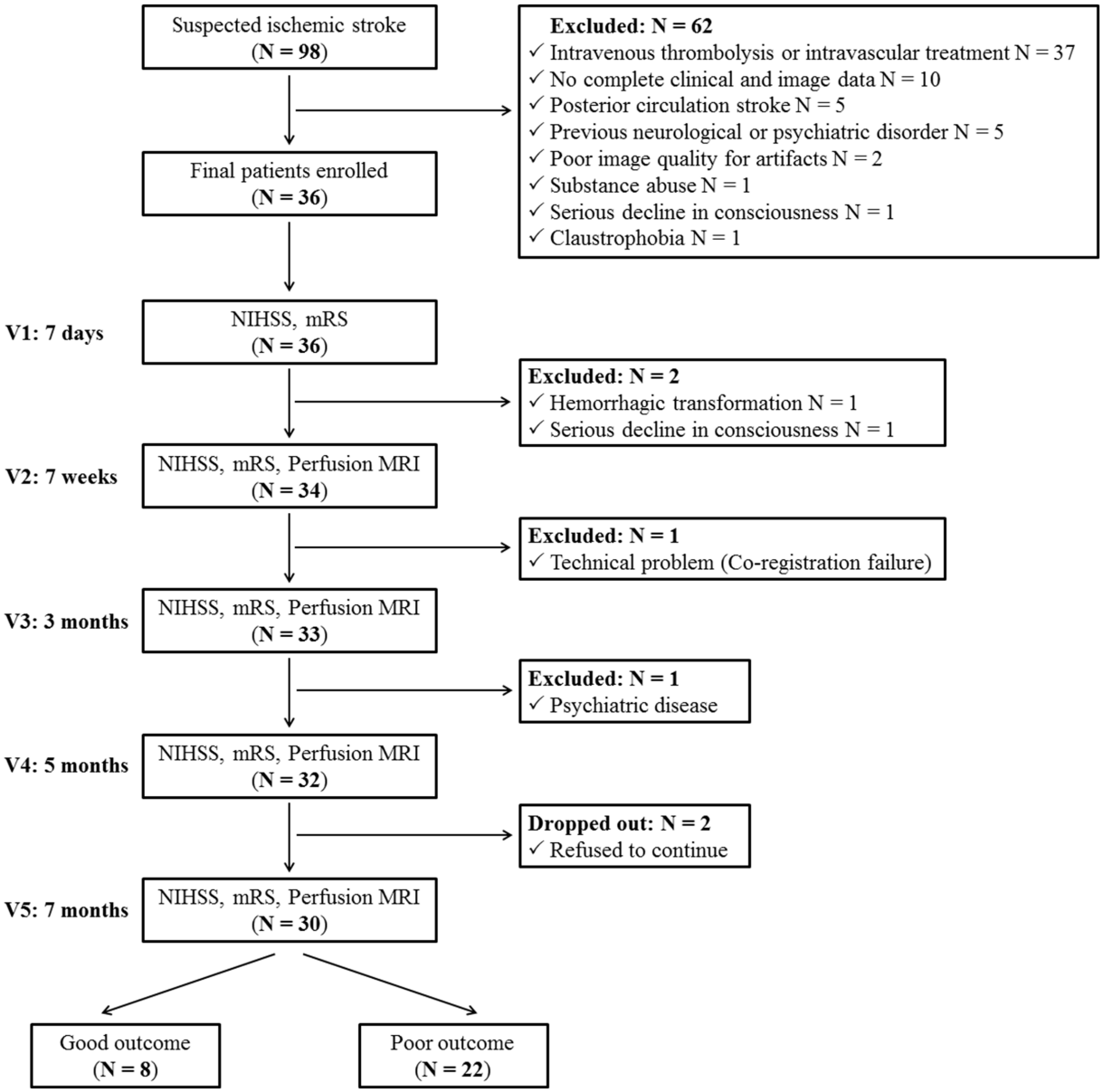

FIGURE 1
Flow chart of the patient enrollment. NIHSS indicates the National Institutes of Health Stroke Scale; mRS: modified Rankin Scale; MRI, magnetic resonance imaging.

FLAIR; matrix: 512 × 512, TR/TE: 11000/125 ms, thickness: 4 mm, gap: 0.4 mm). DWI (matrix: 256 × 256, TR/TE: 2372/55 ms, thickness: 4 mm, gap: 0.4 mm) was performed using an echo-planar imaging (EPI) sequence with $b = 0$ and $b = 1{,}000$ s/mm^2 in three dimensions in space to result in four images per section. Dynamic susceptibility contrast (DSC)-PWI scans (matrix: 130 × 130, TR/TE: 1670/40 ms, thickness: 4 mm, gap: 0 mm, flip angle: 75°) were acquired using a gradient-EPI sequence. A bolus of gadolinium-DOTA (0.2 mmol/kg, Guerbet, Villepinte, France) was injected and flushed with physiological saline (60 mL) at a rate of 5 mL/s with a magnetic resonance-compatible power injector (Medrad, Inc., Warrendale, PA, United States) within 3 seconds at the fifth dynamic scanning of the total fifty scans. To obtain an accurate estimate of the baseline MRI signal intensity S_0 prior to contrast agent injection, an injection delay of 10 s was applied. Eight single-shot, gradient-echo, and echo-planar images were obtained per slice. All sequences were acquired in an axial plane, which was parallel to the anterior–posterior commissures, covering the entire brain.

Data processing

Data analysis was performed using in-house developed modules run in MATLAB (R2016a; The MathWorks, Inc., Natick, MA, United States) and SPM12 free and open source software[1] (Wellcome

1 https://www.fil.ion.ucl.ac.uk/spm/

Trust Centre for NeuroImaging, Inst. of Neurology, University College London, United Kingdom).

DSC–PWI data were analyzed using a parametric approach (Mouridsen et al., 2006). The arterial input function was determined semi-automatically and extracted from a single slice of the PWI scan containing the middle cerebral artery. Maps of the arrival time included time-to-peak (TTP), mean transit time (MTT), and time-to-maximum (T_{max}). TTP was defined as the time point of maximum intensity loss after the passage of the contrast agent. MTT and T_{max} were calculated pixel-wise with a deconvolution approach based on a singular value decomposition using a tracer arrival timing-insensitive method and automatic regularization of oscillations (oscillation index regularized block-circulant singular value decomposition; Schmidt et al., 2020).

Cerebral blood volume (CBV) maps were generated from DSC T2*-weighted images by dynamically tracking the passage of a bolus of a high-susceptibility contrast agent. By detecting the arterial and total tissue concentrations as a function of time during a single transit, the CBV was determined from the ratio of the areas under the tissue and arterial concentration-time curves, respectively, using the following formula:

$$\mathrm{CBV} = \frac{\int_{-\infty}^{\infty} \mathrm{C_t}(\tau)\, d\tau}{\int_{-\infty}^{\infty} \mathrm{C_a}(\tau)\, d\tau}$$

Fieselmann et al. (2011).

To objectively assess differences in lesion blood volume and avoid variations between individuals, the relative cerebral blood volume (rCBV) was estimated using the kinetic analysis of the concentration-time curves after the normalization of CBV because arterial measurements with the limited spatial resolution are not readily quantifiable (Ostergaard, 2005). The CBV maps were normalized to values within the regions contralateral to the stroke lesion with normal-appearing white matter, which were defined to be as large as possible to avoid regions with susceptibility artifacts and partial volume averaging; these were generally normalized to 5%. The MTT was computed from the residue function obtained from the deconvolution, and relative cerebral blood flow (rCBF) was calculated as the ratio rCBV/MTT based on the central volume theorem (Mouridsen et al., 2006).

All image data were registered to T_2 FLAIR images at V2 using mutual information as an objective function and the Nelder–Mead simplex as an optimizer algorithm (deformable co-registration function in SPM12 software), as previously described (He et al., 2017).

Following co-registration, ROIs of ischemia were manually contoured under the guidance of experienced clinicians, including a stroke physician and a neuroradiologist blinded to patient diagnosis. ROIs of the whole stroke lesion were drawn on T_2 FLAIR images, identified as hyperintense regions, and subsequently checked for concordance with DWI images. Caution was taken to exclude the ventricles. The ischemic lesion volume (ILV) was computed by calculating the sum of the lesion areas on each slice. On the contralateral undamaged hemisphere, a mask was applied to delineate an ROI containing normal-appearing white matter with the mean values of each target parameter in healthy tissue (MTT: 5.0 ± 0.9 s; TTP, 23.5 ± 2.3 s; T_{max}, 2.2 ± 0.4 s; rCBF, 16.0 ± 1.7 mL/100 g/min; rCBV, 8.1 ± 0.7%). For each patient, this ROI was used to acquire the range and determine the threshold of each parameter in the PRM analysis. All ROIs (lesion and mirrored reference) were then automatically transferred onto the registered parametric maps of each other, which helped to avoid confusion regarding delineation on non-morphological maps.

Shrinkage or growth of ischemic lesions during stroke development may occur. Under the condition that no significant change was observed in ILV between each pair of time points in the subsequent PRM analysis (V2 vs. V3, V2 vs. V4, and V2 vs. V5), only voxels that were present in both V2 and the other time points were included. Voxels with non-converging fits or values outside the range of validity of the measurement (MTT > 27 s, TTP > 60 s, T_{max} > 60 s, rCBF >100 mL/100 g/min, rCBV >48%) were identified and excluded from the analysis (fractions of all excluded voxels of each map: MTT, 1.0%; TTP, 2.6%; T_{max}, 4.7%; rCBF, 3.0%; rCBV, 3.6%).

Data analysis

Two postprocessing approaches were assessed for monitoring stroke evolution using ROIs delineated on each perfusion parametric map.

Whole-lesion analysis

For each patient at each time point (V2–V5), all parametric perfusion values (MTT, TTP, T_{max}, rCBF, and rCBV) were measured in each ROI.

PRM analysis

Changes in the co-registered perfusion parametric maps were analyzed voxel-wise using PRM for each of the 30 patients at V3, V4, and V5. First, 95% confidence intervals (CIs) were computed based on values from healthy tissues in the mirrored references for the classification of each parametric value. The details of the PRM analytic procedure were described previously (He et al., 2017). The process of the PRM analysis is summarized in Figure 2. After determining each CI (2.8 s for PRM_{MTT}, 4 s for PRM_{TTP}, 2 s for PRM_{Tmax}, 25 mL/100 g/min for PRM_{rCBF}, 1.0% for PRM_{rCBV}) according to the healthy tissue reference, all six parametric maps were obtained at V3, V4, and V5 from comparison with the data acquired at V2 (Figure 3).

Statistical analysis

All statistical analyses were conducted using SPSS software (v26.0; IBM Corp., Armonk, NY, United States). The paired two-tailed Student's *t*-test was used to compare (1) ILV, (2) mean values of each perfusion parameter, and (3) the percentage of voxels with significantly increased or decreased values on each PRM map (PRM_{MTT}, PRM_{TTP}, PRM_{Tmax}, PRM_{rCBF}, and PRM_{rCBV}) between V2 and each other time point. In cases of variance inhomogeneity, the Mann–Whitney test was conducted. The results were expressed as the mean ± standard deviation. The two-sided 5% comparison-wise significance level of a value of $p < 0.05$ was considered statistically significant.

10.3389/fnins.2023.1177044

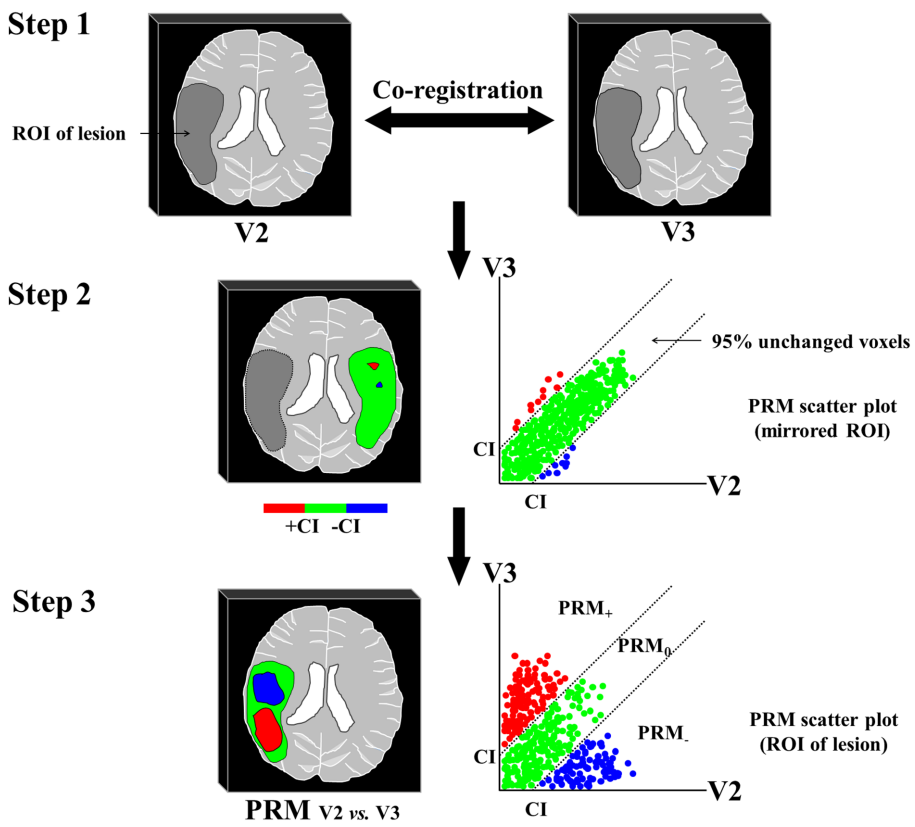

FIGURE 2
Description of the PRM analysis. **Step 1**: MRI data undergo digital image postprocessing that involves co-registration of images for each pair of time points; **Step 2**: The 95% CI for the classification of parametric values is computed based on the lesion-mirrored ROI in the healthy hemisphere. The parametric threshold is determined by the 95% unchanged CI resulting from linear least squares analysis on the combined data from all samples; **Step 3**: PRM maps are determined by calculating the difference between parametric values within the lesion at the pair of time points. PRM maps appear as color-coded overlays on the original parametric maps. Areas with unchanged parametric values are in green, increased values are in red, and decreased values are in blue. The scatter plot represents the two coordinates of a spot and is the parametric value of the same pixel at two-time points. ROI indicates an area of interest; CI, confidence interval; PRM, parametric response mapping; MRI, magnetic resonance imaging.

Receiver operating characteristic (ROC) curve analysis was performed to determine corresponding areas under the curve (AUCs) for significant imaging parameters to predict 7-month mRS scores, aiding the differentiation between good- and poor-outcome subgroups. The Spearman rank-order correlation coefficients indicated the correlation between significant imaging parameters and the clinical readouts at subsequent time points.

Results

Baseline data

Table 1 shows the main demographic and clinical data of the 30 participants. No significant differences were observed in each pair of time points for the NIHSS or mRS scores (both values and rates of change).

Imaging data

At each time point, the mean 3-dimensional ILVs (cm^3) based on the delineated ROIs of the whole sample were measured. No significant differences were observed in ILV measurements between time points. However, while comparing groups, the ILVs of the poor-outcome subgroup at V3 and V5 were significantly larger than those of the good-outcome subgroup at the same time points (V3: 68.7 ± 18.5 vs. 25.2 ± 8.7, $p = 0.002$; V5: 59.8 ± 18.7 vs. 21.4 ± 6.1, $p = 0.005$).

In the whole-lesion analysis approach, the mean MTT and T_{max} values of lesions increased over time, while the mean TTP values remained unchanged. The mean rCBF value decreased over time, while the mean rCBV increased from V2 to V3 and then decreased. No significant differences were observed in the mean values of MTT, TTP, T_{max}, rCBF, and rCBV between the subgroups.

The PRM analysis showed that the fraction of voxels with changes in MTT increased over time, with both increased MTT (PRM_{MTT+}) and decreased MTT (PRM_{MTT-}) following the same pattern in the good-outcome subgroup. The PRM_{MTT+} fractions were similar in both subgroups over time. The PRM_{MTT-} fraction was larger in the poor-outcome subgroup than in the good-outcome subgroup only at V3 (15.0 ± 9.1% vs. 12.8 ± 5.9%), but this was reversed at V4 (15.6 ± 10.3% vs. 16.8 ± 7.0%) and V5 (8.9 ± 6.6% vs. 18.8 ± 6.1%). No significant interactions were observed between the subgroups and time points for PRM_{MTT}. The fraction of voxels with increased TTP (PRM_{TTP+}) and T_{max} (PRM_{Tmax+}) increased over time in both subgroups. The PRM_{TTP+}

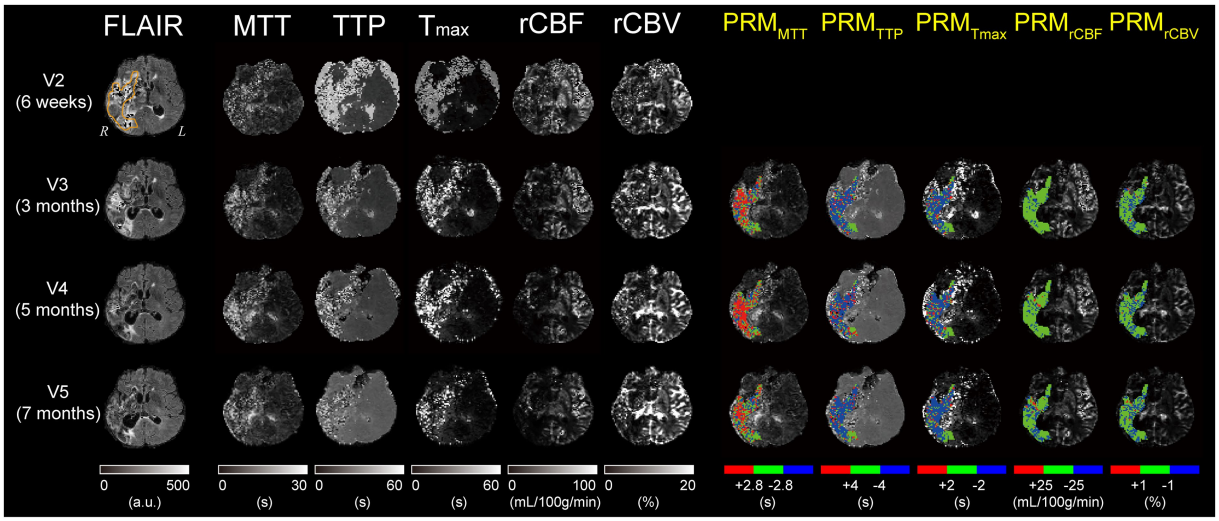

FIGURE 3
Maps of FLAIR, MTT, TTP, T_{max}, rCBF, rCBV at V2-V5, and PRM color-coded maps overlays on MTT, TTP, T_{max}, rCBF, rCBV maps obtained in a representative patient of the poor-outcome subgroup. Each PRM map corresponds to the comparison at V3-V5 with V2. The scale of signal intensity and the threshold for PRM stratification for each map were noted at the end of each column. FLAIR indicates fluid attenuation inversion recovery; MTT, mean transit time; TTP, time-to-peak; T_{max}, time-to-maximum; rCBF, relative cerebral blood flow; rCBV, relative cerebral blood volume; PRM, parametric response mapping; L, left hemisphere; R, right hemisphere.

fractions were similar in the subgroups over time. The PRM_{TTP-} fraction was larger in the poor-outcome subgroup than in the good-outcome subgroup at V3 (28.3 ± 11.1% vs. 20.5 ± 9.8%). At V4, the PRM_{TTP-} fraction was lower, and it was significantly lower in the good-outcome subgroup compared with the poor-outcome subgroup (16.4 ± 5.7% vs. 34.0 ± 7.9%, $p = 0.037$). This was reversed in both subgroups at V5 (22.1 ± 16.2% vs. 24.3 ± 9.4%). The PRM_{Tmax+} fraction was larger in the good-outcome subgroup than in the poor-outcome subgroup at V3 (24.5 ± 9.2% vs. 21.2 ± 7.5%) and V5 (36.3 ± 12.7% vs. 30.7 ± 10.2%), but the opposite was noticed at V4 (25.2 ± 9.8% vs. 27.9 ± 9.6%). The PRM_{Tmax-} fraction was larger in the poor-outcome subgroup than in the good-outcome subgroup at each time point. The PRM_{Tmax} map showed that the voxels with decreased T_{max} values occupied a considerably large fraction of the lesion in the poor-outcome subgroup, as shown in Figure 3. Notably, the PRM_{Tmax-} fraction was significantly lower at V4 in the good-outcome subgroup compared with the poor-outcome subgroup (1.7 ± 1.3% vs. 20.1 ± 13.5%, $p = 0.045$). The fractions of voxels with increased rCBF (PRM_{rCBF+}) were similar in both subgroups at each time point. The PRM_{rCBF-} fraction was larger in the good-outcome subgroup than in the poor-outcome subgroup at V3 (4.1 ± 2.7% vs. 3.7 ± 1.3%), and the opposite was observed at V4 (5.2 ± 2.1% vs. 6.3 ± 2.4%) and V5 (7.2 ± 2.3% vs. 8.0 ± 5.0%). No significant interactions were observed between groups and time points for PRM_{rCBF}. The fraction of voxels with increased rCBV (PRM_{rCBV+}) was significantly larger in the good-outcome subgroup than in the poor-outcome subgroup at V3 (15.7 ± 2.8% vs. 4.7 ± 1.8%, $p = 0.001$), smaller at V4 (6.5 ± 3.9% vs. 9.1 ± 7.2%), and the opposite was noticed at V5 (8.9 ± 4.9% vs. 4.9 ± 2.4%). The fraction of PRM_{rCBV-} was significantly larger in the poor-outcome subgroup than in the good-outcome subgroup at V3 (9.8 ± 2.9% vs. 3.1 ± 1.3%, $p = 0.036$) but not at V4 (10.7 ± 5.1% vs. 7.0 ± 2.7%) or V5 (10.1 ± 3.6% vs. 10.0 ± 4.0%). A color-coded overlay of PRM_{rCBV} from one patient with a good clinical outcome showed sharp differences when compared to that from a patient with a poor clinical outcome. A corresponding quantitative scatter plot demonstrated the distribution of rCBV values at V2 compared with V3 for the entire ILV region. The volume of voxels with increased rCBV values was larger than the volume of voxels with decreased rCBV values in the good-outcome patient compared to the poor-outcome patient at V3. To illustrate the visual intralesional heterogeneity in subgroups with and without favorable functional outcomes, exemplary PRM_{rCBV} maps (with both PRM_{rCBV-} and PRM_{rCBV+} parameters) and corresponding scatter plots are shown in Figure 4.

The ROC analysis was performed using PRM-derived parameters, comparing the mean values at each time point. For the prediction of mRS at V5, PRM_{rCBV-} at V3 had the largest AUC (0.951, $p = 0.002$). When a cutoff of 7.0 for PRM_{rCBV-} was used, the sensitivity and specificity were 0.88 and 1.00, respectively. The PRM_{rCBV+} had the largest AUC (0.864, $p = 0.037$) when a cutoff of 4.0 was applied. The sensitivity and specificity were 0.83 and 0.69, respectively. The ROC curve analysis indicated that PRM_{Tmax-} at V3 could predict mRS scores at V5 and was superior to the mean T_{max} value at V3. For the prediction of mRS scores at V5, PRM_{Tmax-} had the largest AUC (0.912, $p = 0.013$), and the sensitivity and specificity were 0.92 and 0.84, respectively, using a cutoff of 3.1 (Table 2 and Figure 5).

All of the above candidate parameters with potential use in outcome prediction were used in a correlation analysis with both NIHSS and mRS scores at each subsequent time point (Table 3). ILV at V3 was significantly correlated with the NIHSS scores at the same time point ($r = 0.412$, $p < 0.05$). ILV at either time point was not significantly correlated with the functional outcome defined by the 7-month mRS score (mRS at V5). The PRM_{rCBV-} at V3 was significantly correlated with both NIHSS and mRS scores at V5 (NIHSS: $r = 0.524$, $p < 0.05$; mRS: $r = 0.610$, $p < 0.01$). PRM_{rCBV+} at V3 was inversely correlated with mRS scores at V5 ($r = -0.668$, $p < 0.01$) and with

TABLE 1 Baseline characteristics and clinical information of 30 patients with chronic stroke.

	All patients (*n*=30)	Good-outcome (*n*=8)	Poor-outcome (*n*=22)
Age (years), mean ± SD	51.5 ± 10.3	49.8 ± 11.7	52.2 ± 9.6
Gender, men/women, *n* (%)	21/9 (70.0/30.0)	7/1 (87.5/12.5)	14/8 (63.6/36.4)
Vascular risk factor			
Diabetes mellitus, *n* (%)	3 (10.0)	1 (12.5)	2 (9.1)
Hypertension, *n* (%)	12 (40.0)	4 (50.0)	8 (36.4)
Hyperlipidemia, *n* (%)	7 (23.3)	2 (25.0)	5 (22.7)
Atrial fibrillation, *n* (%)	5 (16.7)	1 (12.5)	4 (18.2)
Coronary artery disease, *n* (%)	3 (10.0)	1 (12.5)	2 (9.1)
Current smoking, *n* (%)	9 (30.0)	1 (12.5)	8 (36.4)
Clinical parameters			
Lesion side, right/left hemisphere, *n* (%)	21/9 (70.0/30.0)	5/3 (62.5/37.5)	16/6 (72.7/27.3)
Infarct arterial territory, MCA, *n* (%)	25 (83.3)	5 (62.5)	20 (90.9)
NIHSS (RC), mean ± SD (%)			
V1: 7 days	16.4 ± 4.0	12.6 ± 2.2	17.7 ± 3.7
V2: 6 weeks	12.1 ± 5.2 (10.1 ± 3.6)	7.4 ± 2.4 (10.3 ± 1.7)	13.7 ± 4.9 (9.9 ± 1.6)
V3: 3 months	10.5 ± 4.4 (4.5 ± 1.1)	5.9 ± 1.8 (3.5 ± 1.5)	12.1 ± 3.8 (5.0 ± 1.5)
V4: 5 months	10.0 ± 4.4 (2.0 ± 0.3)	5.8 ± 2.0 (3.1 ± 0.8)	11.5 ± 4.0 (1.4 ± 0.2)
V5: 7 months	9.1 ± 4.8 (2.9 ± 0.5)	4.5 ± 2.1 (4.0 ± 1.0)	10.7 ± 4.5 (2.3 ± 0.5)
mRS (RC), mean ± SD (%)			
V1: 7 days	4.0 ± 0.7	3.3 ± 0.6	4.3 ± 0.4
V2: 6 weeks	3.7 ± 0.7 (1.1 ± 0.3)	3.1 ± 0.7 (1.3 ± 0.5)	3.9 ± 0.6 (1.0 ± 0.3)
V3: 3 months	3.3 ± 0.7 (1.0 ± 0.2)	2.8 ± 0.8 (0.9 ± 0.4)	3.5 ± 0.6 (1.0 ± 0.3)
V4: 5 months	3.0 ± 0.5 (0.5 ± 0.1)	2.5 ± 0.5 (0.5 ± 0.2)	3.2 ± 0.4 (0.5 ± 0.2)
V5: 7 months	2.8 ± 0.7 (0.2 ± 0.1)	1.8 ± 0.4 (0.2 ± 0.1)	3.2 ± 0.4 (0.0 ± 0.0)

All data are displayed as mean ± standard deviation (SD) or *n* (%). MCA indicates middle cerebral artery; NIHSS, National Institutes of Health Stroke Scale; mRS, modified Rankin Scale; RC, rate of change, which is calculated by the ratio of the absolute value of measure difference between two continuous time points to the value at the previous time point (e.g., RC of NIHSS at V5 = $|NIHSS_{V4} - NIHSS_{V5}|/NIHSS_{V4}$).

NIHSS scores at V4 and V5 ($r=-0.583$, $p<0.05$; $r=-0.518$, $p<0.05$, respectively). Furthermore, $PRM_{Tmax\text{-}}$ at V3 was significantly correlated with both NIHSS and mRS scores at V4 (NIHSS: $r=0.571$, $p<0.01$; mRS: $r=0.593$, $p<0.01$) and at V5 (NIHSS: $r=0.640$, $p<0.01$; mRS: $r=0.621$, $p<0.01$); it also correlated with the rate of change of mRS score at V5 ($r=0.534$, $p<0.05$). The mean T_{max} estimated using the whole-lesion approach at each early time point was not correlated with NIHSS or mRS scores at V5. Since NIHSS and mRS scores at V5 were significantly correlated ($r=0.744$, $p<0.01$) but the $PRM_{rCBV\text{-}}$ was not correlated with PRM_{rCBV+} at V3 ($r=0.279$, $p>0.05$), both PRM_{rCBV} metrics should be regarded as independent predictors for long-term clinical outcomes. Finally, $PRM_{rCBV\text{-}}$, PRM_{rCBV+}, and $PRM_{Tmax\text{-}}$ were chosen as predictive imaging biomarkers for final mRS scores.

Discussion

It has been reported that 24-h and 1-week ILVs were strongly associated with functional outcomes 3 months after stroke (Bucker et al., 2017). The results of the present study showed significant differences between the 3-month and 7-month ILVs (ILV at V3 and V5) between outcome subgroups. However, based on ROC and correlation analyses, the 3-month ILV showed a weak ability to predict further functional outcomes, and no significant correlation was found between the 3-month ILV and 7-month mRS scores. We hypothesized that the ILV in patients with chronic stroke may reflect current patient status but not predict final functional outcomes.

In the present study, a reduction in ILVs instead of growth was found over time in both subgroups. Close attention should be paid to the heterogeneity of lesions during stroke development. Inconsistencies regarding post-stroke prognosis have been reported in some clinical studies that focused on patients with infarctions of similar sizes, impaired arterial territory, and duration after symptom onset (Koyama et al., 2014; Lima et al., 2014; de Peretti et al., 2018; Tian et al., 2021). Possible explanations for this diversity in clinical outcomes have been proposed and include interindividual differences in collateral circulation, preconditioning, and microcirculation responses after ischemic impairment (Thompson et al., 2013; Malik et al., 2014; Winship, 2015; Rost and Brodtmann, 2022). The cerebral collateral circulation is an evolutionarily conserved blood vessel network that maintains consistent cerebral perfusion when encountering physiological or pathophysiological changes in hemodynamics (Sohn et al., 2016). The clinical progression of patients with chronic stroke can be evaluated using the status of collateral circulation in terms of the risk of stroke recurrence. The state of the collateral flow networks was significantly correlated with the follow-up status of patients with stroke (Yao et al., 2018; Liu X. et al., 2022; Liu Y. et al., 2022). The evaluation of cerebral collateral circulation can be accomplished using real-time non-invasive imaging techniques, including perfusion MRI (Ong et al., 2019). Previous clinical studies using perfusion MRI for stroke monitoring have evaluated the abilities of different types of MRI sequences or parameters, both morphological and quantitative, as potential predictors of clinical outcomes. However, most of these studies have relied on whole-lesion mean values for summary statistics of multiparametric MRI maps for the quantification of corresponding parameters, showing varying clinical significance (Kufner et al., 2021). Polytropic changes in parametric values throughout lesions were believed to desensitize the results using the whole-lesion approach. In the present study, spatial information was preserved using PRM, and local variations in terms of all voxels with changed or relatively stable values during stroke evolution could

10.3389/fnins.2023.1177044

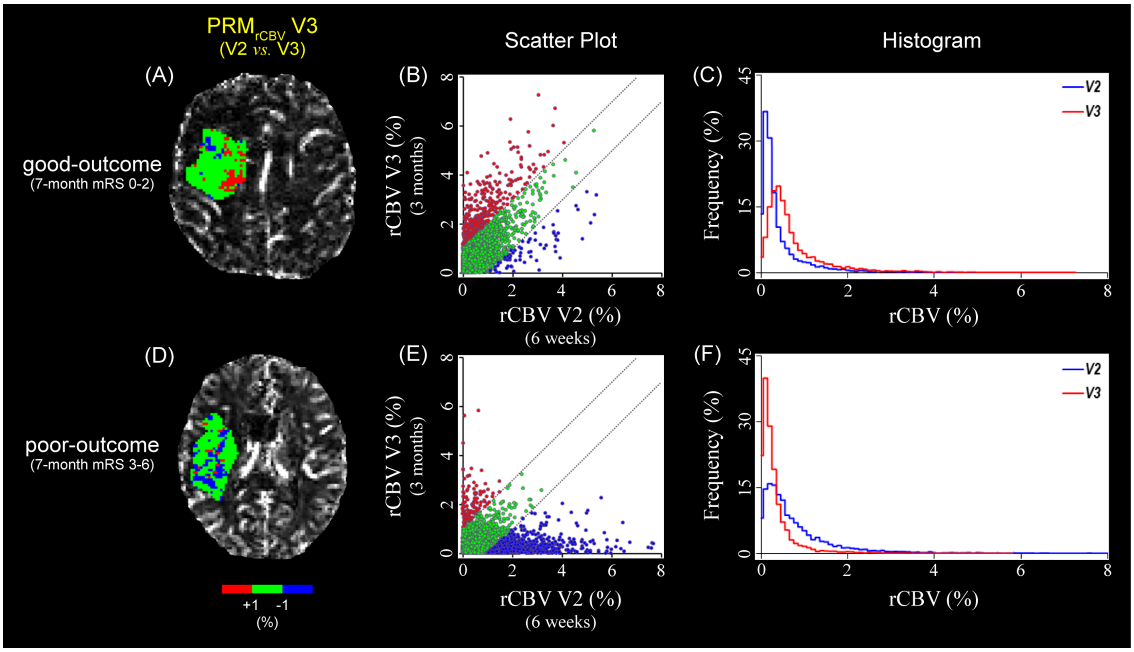

FIGURE 4
The PRM_{rCBV} color-coded overlay, the corresponding quantitative scatter plot, and the histogram of a representative patient in the good-outcome subgroup compared to the representations of one in the poor-outcome subgroup. **(A,E)** The regions in which rCBV values were significantly increased (red voxels), unchanged (green voxels), or significantly decreased (blue voxels) based on the predetermined threshold (CI=1.0%) were represented in a color-coded overlay. **(B,D)** The scatter plots showed the distribution of rCBV at V2 and V3 for the entire 3-D lesion volume. The 95% CIs within the scatter plot were designated by two black dashed lines. **(C,F)** The histogram represented the grouped frequency distribution of rCBV. PRM indicates parametric response mapping; CI, confidence interval; rCBV, relative cerebral blood volume.

TABLE 2 The performance of 3-month imaging parameters in predicting the 7-month mRS.

Parameters at V3 (3 months)	Youden index	Cutoff value	AUC	95% CIs	Sensitivity (%)	Specificity (%)	Value of *p*
PRM_{rCBV-}	0.88	7.00	0.951	0.881–0.990	88	100	0.002**
PRM_{rCBV+}	0.52	4.00	0.864	0.853–0.944	83	69	0.037*
PRM_{Tmax-}	0.75	3.10	0.912	0.790–0.982	92	83	0.013*
ILV	0.22	52.24	0.681	0.574–0.770	55	67	0.190
Mean rCBV	0.18	6.20	0.650	0.581–0.690	64	54	0.262
Mean T_{max}	0.16	4.70	0.634	0.574–0.670	54	62	0.377

PRM indicates parametric response mapping; rCBV, relative cerebral blood volume; T_{max}, time-to-maximum; ILV, ischemic lesion volume; AUC, area under the curve; CI, confidence interval; mRS, modified Rankin Scale. *$p < 0.05$; **$p < 0.01$: A difference in comparison with the performance with AUC = 0.5.

be distinguished based on their spatial distributions. Furthermore, the relationship between quantitative heterogeneous changes in multiparametric MRI maps and functional outcomes has not been widely addressed in clinical settings, though this has been suggested in preclinical studies (Lestro Henriques et al., 2015; Wang et al., 2020; Kang et al., 2021).

In the present study, no specific therapy was performed during post-stroke follow-up, and the correlation between the PRM results and final functional outcomes can be considered a key influencer of the individual inhomogeneity of stroke development in different patients, which may be hidden in whole-lesion analytic methods. These new findings revealed that, using PRM, highlights the importance of heterogeneity in chronic stroke, which may lead to different clinical outcomes.

Relative CBV is an important perfusion parameter corresponding to the volume of blood passing through the capillary networks contained in a certain volume of the brain (Kaneko et al., 2004). An area suffering from ischemia with normal blood flow and delayed arrival time indices generally shows that regional blood supply is maintained by autoregulation, but this effect occurs late in the potential infarct core area and is temporarily sustained by collaterals. In general, the volume of brain areas with decreased rCBV caused by capillary obstruction or metabolic depression correlates well with the final infarction size. Several factors, including plugging of capillaries by leukocytes, endothelial swelling, formation of microvilli, platelet aggregation, and external compression of capillaries secondary to edema or perivascular astrocyte swelling, contribute to rCBV reduction (Chamorro, 2007). Particularly, when delayed arrival time

was observed in areas with decreased rCBV, it might imply insufficient collateral circulation in the focal brain tissue, which could eventually evolve into an infarction (Singer et al., 2003; Lee et al., 2009; Kim et al., 2014; Provost et al., 2019). In the example of PRM color-coded overlays in a poor-outcome patient (Figure 3), the spatial distribution of the blue layer in the PRM_{rCBV} map (PRM_{rCBV-}) matched that of the red layer in the PRM_{MTT} map (PRM_{MTT+}), supporting this theory in chronic stroke.

In the present study, the percentage changes in rCBV defined using PRM at V3 outperformed single mean rCBV values in determining both long-term neurological and functional outcomes after stroke. The mean rCBV value at V3 did not correlate with further prognosis or sufficiently stratify the patients with different clinical outcomes. The predictive capability of PRM_{rCBV} was also confirmed by the ROC analysis. A possible explanation was that the reduction in the local blood volume in brain tissue that occurred over 7 weeks (from V2 to V3) might portend an unfavorable long-term outcome owing to poor collateral circulation, which is in accordance with previous studies (Park et al., 2011, 2014).

The PRM_{rCBV} map provided details on perfusion, which might provide information on the quality and quantity of collateral flow. However, increased PRM_{rCBV-} or decreased PRM_{rCBV+} at V3 correlated with high NIHSS or mRS scores at V5 and cannot be simply interpreted as a lower total value of rCBV correlating with poor clinical outcomes. An increase in PRM_{rCBV+} or a decrease in PRM_{rCBV-} in chronic stroke may be derived from an increase in the overall microvasculature density or dilation of microvessels, as both could lead to a net increase in cerebral blood volume in ischemic regions. Correlation analysis showed that PRM_{rCBV-} was not correlated with PRM_{rCBV+} at V3, which meant that either parameter could be used as an independent predictor of long-term clinical outcomes.

In perfusion MRI, T_{max} represents the time from the start of the scan until the maximum intensity of the contrast agent arrives at each voxel. This value is sensitive to the residual function of brain tissue in infarction and changes in perfusion. T_{max} can also predict brain tissue viability after ischemic injury, and high T_{max} values have been correlated with a lower likelihood of tissue survival (Shih et al., 2003; Olivot et al., 2009a,b). T_{max} may be increased in large volumes of tissue that do not proceed to infarction, regardless of CBF status (Bang et al., 2010; Lee et al., 2015). Since T_{max} is not influenced by scan duration, sufficient scanning for a long time is possible to achieve an even distribution of the contrast agent (Copen et al., 2011). In addition, T_{max} has little gray matter/white matter heterogeneity and a relatively low number of large blood vessels, which may complicate the observation of the parenchymal condition. It has also been speculated as a measure of the extent of collateral circulation (Giammello et al., 2022; Gwak et al., 2022). Thus, T_{max} is considered a widely accepted, reliable perfusion parameter to assess tissue viability in stroke, but the exact threshold remains controversial. In previous studies, different thresholds for T_{max} have been set with the main goal of accurately representing the situation of acute stroke development, although this parameter has been seldom used in cases of chronic stroke. In the evaluation of the effects of alteplase injection beyond 3 h after stroke onset in

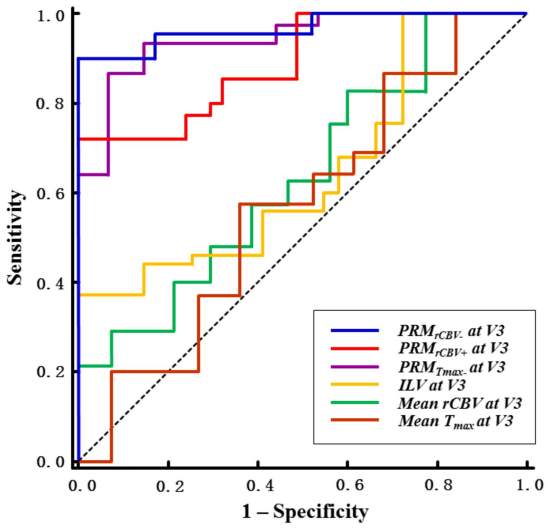

FIGURE 5
Receiver operating characteristic (ROC) curve of PRM-derived parameters and mean values for predicting the final mRS score. The best diagnostic performance of PRM-derived parameters for predicting the mRS at V5 could be achieved with PRM_{rCBV-} at V3 with 7.0% as the cutoff value (AUC: 0.951; sensitivity: 0.88; specificity: 1.00). PRM_{rCBV+} and PRM_{Tmax-} at V3 also performed well in predicting the mRS at V5. The dashed line indicates a curve with no discrimination. ROC indicates receiver-operating characteristic; PRM, parametric response mapping; mRS, modified Rankin Scale; AUC, area under the curve; ILV, ischemic lesion volume; rCBV, relative cerebral blood volume; T_{max}, time-to-maximum.

TABLE 3 Spearman rank-order correlation coefficients of the potential predictors in ROC curve analyses.

		mRS V5	mRS V4	NIHSS V5	NIHSS V4	RC of mRS V5	RC of mRS V4	RC of NIHSS V5	RC of NIHSS V4
PRM_{rCBV-} V3	*r*	0.610	0.521	0.524	0.464	0.556	0.407	0.537	0.609
	p	0.009**	0.077	0.037*	0.092	0.086	0.101	0.171	0.128
PRM_{rCBV+} V3	*r*	−0.668	−0.514	−0.518	−0.583	−0.654	−0.601	−0.676	−0.624
	p	0.005**	0.086	0.040*	0.018*	0.067	0.170	0.390	0.287
PRM_{Tmax-} V3	*r*	0.621	0.593	0.640	0.571	0.534	0.455	0.510	0.497
	p	0.003**	0.006**	0.001**	0.003**	0.022*	0.224	0.200	0.604

PRM indicates parametric response mapping; rCBV, relative cerebral blood volume; T_{max}, time-to-maximum; NIHSS, National Institutes of Health Stroke Scale; mRS, modified Rankin Scale; RC, rate of change (e.g., RC of mRS at V5 = $|mRS_{V4} - mRS_{V5}|/mRS_{V4}$); ROC, receiver-operating characteristic; V3: 3 months; V4: 5 months; V5: 7 months. *$p < 0.05$; **$p < 0.01$ (statistically significant).

the Echoplanar Imaging Thrombolytic Evaluation Trial cohort, a T_{max} of 4–6 s delay was used (Donnan et al., 2009; Olivot et al., 2009a,b). A T_{max} of >8 s with a core volume of approximately 100 mL (lesion size on DWI) was reported as an adequate threshold for the identification of patients with malignant profiles of infarction and consequently unfavorable functional outcomes despite reperfusion therapy (Giammello et al., 2022). A T_{max} of ≥10 s was also reported in another study to better predict the final infarction volume (Fainardi et al., 2022).

Generally, optimal T_{max} thresholds from one study must be used with caution in other studies if the same observation conditions are not ensured. However, PRM analysis is an objective assessment based on intraindividual percentage changes of complementary temporal and spatial information and avoids the bias of threshold setting among different studies. Using conventional analytic methods, an increasing number of studies have promoted the use of T_{max} in clinical trials (Albers et al., 2006; Davis et al., 2008; Olivot et al., 2009a,b). However, various hemodynamic situations may result in the same T_{max} measurements. In addition to the influence of deconvolution, other factors, such as arterial abnormalities, also lead to bolus temporal dispersion, affecting the measurement of T_{max} (Calamante et al., 2006). One study showed that, while T_{max} theoretically reflects bolus delay, it is also influenced by bolus temporal dispersion and, to a lesser degree, by MTT (Ford et al., 2014). Primarily, T_{max} and MTT both reflect macrovascular features (Calamante et al., 2010). Nevertheless, T_{max} abnormalities could not be solely explained by prolonged MTT; they should be considered with the combination of other macrovascular or microvascular indices to interpret physiological processes so that the various factors contributing to the measured T_{max} may be disentangled. Due to the complex interactions between different factors influencing T_{max}, the clinical significance of T_{max} is not straightforward. To have a reasonable and objective understanding of the significance of delay-weighted measures in chronic stroke, the temporal dynamics of the blood supply, including collateral circulation recruitment, are required to provide more information based on delay-related perfusion parameters (Liebeskind, 2005; Christensen et al., 2008). Coincidentally, the PRM approach is able to indicate the temporal evolution of all voxel-wise parameters and may help explain the relevance of T_{max} in post-stroke pathophysiology.

Among the perfusion parameters based on arrival time in the present study, the 3-month PRM_{Tmax-} (at V3) could best reflect the current clinical status and predict both 7-month NIHSS and mRS scores in patients with chronic stroke. Because this was positively correlated with both clinical outcome scores at two continuous time points, the significantly shortened T_{max} during the follow-up from V2 to V3 may imply unfavorable neurological and functional deficits. The ROC analysis also confirmed that the predictive capability of PRM_{Tmax-} was superior to the mean T_{max} with high sensitivity and specificity.

In the present study, the PRM approach showed some improvement in assessing clinical outcomes in patients with chronic stroke in the present study, but there were also some limitations. The challenge of validation of all components of this approach still remains, including patient enrollment, imaging data acquisition, algorithm selection for co-registration, and response mapping for heterogeneity illustration and interpretation (Boes et al., 2014; Duering et al., 2020). Due to problems associated with technical processing, an overall influence of the image datasets emerged. The sample size of the PRM analysis was small because of failures in co-registration between time points, possibly induced by susceptibility artifacts. Consistent imaging protocols that provide repeatable and quantitative readouts are crucial for applying PRM across clinical settings. However, the predictive potential of PRM for clinical outcomes in patients with stroke has been evaluated using ROC analysis. To obtain objective sensitivity in ROC curve analysis, various PRM cutoff values should be tested using large sample sizes. Moreover, associations between imaging readouts and functional outcomes defined as a certain mRS score should be assessed. Future studies should focus on applicability across imaging parameters or even modalities in a repeatable and robust manner. The design of PRM studies should be individualized and targeted based on the pathophysiological characteristics of disease progression.

Conclusion

The present study described the first clinical application of PRM analysis using multiparametric MRI measures based on perfusion maps in chronic stroke. PRM_{rCBV-}, PRM_{rCBV+}, and PRM_{Tmax-}, as perfusion MRI parameters analyzed using PRM, possessed strong predictive power for clinical outcomes in patients with chronic stroke. These parameters were also highly correlated with the final mRS scores, which concern long-term functional impairment and the degree of disability, and the conventional whole-lesion output data were not correlated with these scores. This novel approach allows for spatial voxel-wise tracking of hemodynamics using imaging data. In the monitoring of patients with chronic stroke, it may be feasible to use perfusion MRI PRM metrics as imaging biomarkers for prognosis. With the existing superiority of PRM applications in voxel-based tracking of stroke status and progression, it may be more suitable to reflect the pathophysiological heterogeneity within ischemic lesions and provide a new perspective for the assessment of stroke evolution. This can also be a promising tool for evaluating therapeutic effects in greater detail when new therapies are developed for the treatment of stroke.

Data availability statement

The original contributions presented in the study are included in the article/supplementary material, further inquiries can be directed to the corresponding author.

Ethics statement

The studies involving human participants were reviewed and approved by The Institutional Review Board of Shanghai Sixth People's Hospital Affiliated to Shanghai Jiao Tong University School of Medicine, Shanghai, China. The ethics committee waived the requirement of written informed consent for participation.

Author contributions

RH, JZ, and YL: conception and design of the study. RH, JZ, and XX: acquisition and analysis of the data. RH, JZ, and XW: verification of analytic approach. RH and XW: data interpretation and statistical analysis. RH, JZ, and FW: draft of a significant portion of the manuscript or figures. RH and YL: review, editing, and submitted work. YL: project administration and supervision. All authors approved the final version of the manuscript.

Funding

This program was sponsored by the Interdisciplinary Program of Shanghai Jiao Tong University (YQ2019QNA22 and YQ2021QN95) and Shanghai Key Clinical Specialty (No. shslczdzk03203).

Conflict of interest

The authors declare that the research was conducted in the absence of any commercial or financial relationships that could be construed as a potential conflict of interest.

Publisher's note

References

Albers, G. W., Thijs, V. N., Wechsler, L., Kemp, S., Schlaug, G., Skalabrin, E., et al. (2006). Magnetic resonance imaging profiles predict clinical response to early reperfusion: the diffusion and perfusion imaging evaluation for understanding stroke evolution (DEFUSE) study. *Ann. Neurol.* 60, 508–517. doi: 10.1002/ana.20976

Audebert, H. J., and Fiebach, J. B. (2015). Brain imaging in acute ischemic stroke—MRI or CT? *Curr. Neurol. Neurosci. Rep.* 15:6. doi: 10.1007/s11910-015-0526-4

Baer, A. H., Hoff, B. A., Srinivasan, A., Galban, C. J., and Mukherji, S. K. (2015). Feasibility analysis of the parametric response map as an early predictor of treatment efficacy in head and neck cancer. *AJNR Am. J. Neuroradiol.* 36, 757–762. doi: 10.3174/ajnr.A4296

Bang, O. Y., Lee, K. H., Kim, S. J., and Liebeskind, D. S. (2010). Benign oligemia despite a malignant MRI profile in acute ischemic stroke. *J. Clin. Neurol.* 6, 41–45. doi: 10.3988/jcn.2010.6.1.41

Banks, J. L., and Marotta, C. A. (2007). Outcomes validity and reliability of the modified Rankin scale: implications for stroke clinical trials: a literature review and synthesis. *Stroke* 38, 1091–1096. doi: 10.1161/01.STR.0000258355.23810.c6

Boes, J. L., Hoff, B. A., Hylton, N., Pickles, M. D., Turnbull, L. W., Schott, A. F., et al. (2014). Image registration for quantitative parametric response mapping of cancer treatment response. *Transl. Oncol.* 7, 101–110. doi: 10.1593/tlo.14121

Bucker, A., Boers, A. M., Bot, J. C. J., Berkhemer, O. A., Lingsma, H. F., Yoo, A. J., et al. (2017). Associations of ischemic lesion volume with functional outcome in patients with acute ischemic stroke: 24-hour versus 1-week imaging. *Stroke* 48, 1233–1240. doi: 10.1161/strokeaha.116.015156

Calamante, F., Christensen, S., Desmond, P. M., Ostergaard, L., Davis, S. M., and Connelly, A. (2010). The physiological significance of the time-to-maximum (Tmax) parameter in perfusion MRI. *Stroke* 41, 1169–1174. doi: 10.1161/strokeaha.110.580670

Calamante, F., Willats, L., Gadian, D. G., and Connelly, A. (2006). Bolus delay and dispersion in perfusion MRI: implications for tissue predictor models in stroke. *Magn. Reson. Med.* 55, 1180–1185. doi: 10.1002/mrm.20873

Chamorro, A. (2007). Magnetic resonance perfusion diffusion mismatch, thrombolysis, and clinical outcome in acute stroke. *J. Neurol. Neurosurg. Psychiatry* 78:443. doi: 10.1136/jnnp.2006.108795

Cho, N., Im, S. A., Park, I. A., Lee, K. H., Li, M., Han, W., et al. (2014). Breast cancer: early prediction of response to neoadjuvant chemotherapy using parametric response maps for MR imaging. *Radiology* 272, 385–396. doi: 10.1148/radiol.14131332

Christensen, S., Calamante, F., Hjort, N., Wu, O., Blankholm, A. D., Desmond, P., et al. (2008). Inferring origin of vascular supply from tracer arrival timing patterns using bolus tracking MRI. *J. Magn. Reson. Imaging* 27, 1371–1381. doi: 10.1002/jmri.21386

Copen, W. A., Schaefer, P. W., and Wu, O. (2011). MR perfusion imaging in acute ischemic stroke. *Neuroimaging Clin. N. Am.* 21, 259–83, x. doi: 10.1016/j.nic.2011.02.007

Davis, S. M., Donnan, G. A., Parsons, M. W., Levi, C., Butcher, K. S., Peeters, A., et al. (2008). Effects of alteplase beyond 3 h after stroke in the Echoplanar imaging thrombolytic evaluation trial (EPITHET): a placebo-controlled randomised trial. *Lancet Neurol.* 7, 299–309. doi: 10.1016/S1474-4422(08)70044-9

de Peretti, C., Gabet, A., Lecoffre, C., Oberlin, P., Olié, V., and Woimant, F. (2018). Regional disparities in acute and post-acute care of stroke patients in France, 2015. *Rev. Neurol.* 174, 555–563. doi: 10.1016/j.neurol.2017.09.014

Donnan, G. A., Baron, J. C., Ma, H., and Davis, S. M. (2009). Penumbral selection of patients for trials of acute stroke therapy. *Lancet Neurol.* 8, 261–269. doi: 10.1016/s1474-4422(09)70041-9

Duering, M., Adam, R., Wollenweber, F. A., Bayer-Karpinska, A., Baykara, E., and Cubillos-Pinilla, L. Y. (2020). Within-lesion heterogeneity of subcortical DWI lesion evolution, and stroke outcome: a voxel-based analysis. *J. Cereb. Blood Flow Metab.* 40, 1482–1491. doi: 10.1177/0271678x19865916

Fainardi, E., Busto, G., Rosi, A., Scola, E., Casetta, I., Bernardoni, A., et al. (2022). T(max) volumes predict final infarct size and functional outcome in ischemic stroke patients receiving endovascular treatment. *Ann. Neurol.* 91, 878–888. doi: 10.1002/ana.26354

Fieselmann, A., Kowarschik, M., Ganguly, A., Hornegger, J., and Fahrig, R. (2011). Deconvolution-based CT and MR brain perfusion measurement: theoretical model revisited and practical implementation details. *Int. J. Biomed. Imaging.* 2011:467563, 1–20. doi: 10.1155/2011/467563

Ford, A. L., An, H., Kong, L., Zhu, H., Vo, K. D., Powers, W. J., et al. (2014). Clinically relevant reperfusion in acute ischemic stroke: MTT performs better than Tmax and TTP. *Transl. Stroke Res.* 5, 415–421. doi: 10.1007/s12975-014-0325-2

Galbán, C. J., Chenevert, T. L., Meyer, C. R., Tsien, C., Lawrence, T. S., Hamstra, D. A., et al. (2009). The parametric response map is an imaging biomarker for early cancer treatment outcome. *Nat. Med.* 15, 572–576. doi: 10.1038/nm.1919

Galbán, C. J., Han, M. K., Boes, J. L., Chughtai, K. A., Meyer, C. R., Johnson, T. D., et al. (2012). Computed tomography-based biomarker provides unique signature for diagnosis of COPD phenotypes and disease progression. *Nat. Med.* 18, 1711–1715. doi: 10.1038/nm.2971

Giammello, F., De Martino, S. R. M., Simonetti, L., Agati, R., Battaglia, S., Cirillo, L., et al. (2022). Predictive value of Tmax perfusion maps on final core in acute ischemic stroke: an observational single-center study. *Radiol. Med.* 127, 414–425. doi: 10.1007/s11547-022-01467-8

Gwak, D. S., Choi, W., Kwon, J. A., Shim, D. H., Kim, Y. W., and Hwang, Y. H. (2022). Perfusion profile evaluated by severity-weighted multiple Tmax strata predicts early neurological deterioration in minor stroke with large vessel occlusion. *J. Cereb. Blood Flow Metab.* 42, 329–337. doi: 10.1177/0271678x211029165

Hamstra, D. A., Galban, C. J., Meyer, C. R., Johnson, T. D., Sundgren, P. C., Tsien, C., et al. (2008). Functional diffusion map as an early imaging biomarker for high-grade glioma: correlation with conventional radiologic response and overall survival. *J. Clin. Oncol.* 26, 3387–3394. doi: 10.1200/JCO.2007.15.2363

He, R., Moisan, A., Detante, O., Remy, C., Krainik, A., Barbier, E. L., et al. (2017). Evaluation of parametric response mapping to assess therapeutic response to human mesenchymal stem cells after experimental stroke. *Cell Transplant.* 26, 1462–1471. doi: 10.1177/0963689717721211

Hendrix, P., Melamed, I., Collins, M., Lieberman, N., Sharma, V., Goren, O., et al. (2022). NIHSS 24 h after mechanical Thrombectomy predicts 90-day functional outcome. *Clin. Neuroradiol.* 32, 401–406. doi: 10.1007/s00062-021-01068-4

Kaneko, K., Kuwabara, Y., Mihara, F., Yoshiura, T., Nakagawa, M., Tanaka, A., et al. (2004). Validation of the CBF, CBV, and MTT values by perfusion MRI in chronic occlusive cerebrovascular disease: a comparison with 15O-PET. *Acad. Radiol.* 11, 489–497. doi: 10.1016/s1076-6332(03)00722-0

Kang, M., Jin, S., and Cho, H. (2021). MRI investigation of vascular remodeling for heterogeneous edema lesions in subacute ischemic stroke rat models: correspondence between cerebral vessel structure and function. *J. Cereb. Blood Flow Metab.* 41, 3273–3287. doi: 10.1177/0271678x211029197

Kim, B. J., Kang, H. G., Kim, H. J., Ahn, S. H., Kim, N. Y., Warach, S., et al. (2014). Magnetic resonance imaging in acute ischemic stroke treatment. *J. Stroke*. 16, 131–145. doi: 10.5853/jos.2014.16.3.131

König, I. R., Ziegler, A., Bluhmki, E., Hacke, W., Bath, P. M., Sacco, R. L., et al. (2008). Predicting long-term outcome after acute ischemic stroke: a simple index works in patients from controlled clinical trials. *Stroke* 39, 1821–1826. doi: 10.1161/strokeaha.107.505867

Koyama, T., Marumoto, K., Miyake, H., and Domen, K. (2014). Relationship between diffusion tensor fractional anisotropy and long-term motor outcome in patients with hemiparesis after middle cerebral artery infarction. *J. Stroke Cerebrovasc. Dis.* 23, 2397–2404. doi: 10.1016/j.jstrokecerebrovasdis.2014.05.017

Kufner, A., Khalil, A. A., Galinovic, I., Kellner, E., Mekle, R., and Rackoll, T. (2021). Magnetic resonance imaging-based changes in vascular morphology and cerebral perfusion in subacute ischemic stroke. *J. Cereb. Blood Flow Metab.* 41, 2617–2627. doi: 10.1177/0271678X211010071

Lee, S. Y., Cha, J. K., and Kang, M. J. (2009). Regional cerebral blood volume ratio on perfusion MRI on the growth of infarct size in acute ischemic stroke. *Eur. Neurol.* 62, 281–286. doi: 10.1159/000235597

Lee, M. J., Son, J. P., Kim, S. J., Ryoo, S., Woo, S. Y., Cha, J., et al. (2015). Predicting collateral status with magnetic resonance perfusion parameters: probabilistic approach with a Tmax-derived prediction model. *Stroke* 46, 2800–2807. doi: 10.1161/strokeaha.115.009828

Lestro Henriques, I., Gutierrez-Fernandez, M., Rodriguez-Frutos, B., Ramos-Cejudo, J., Otero-Ortega, L., Navarro Hernanz, T., et al. (2015). Intralesional patterns of MRI ADC maps predict outcome in experimental stroke. *Cerebrovasc. Dis.* 39, 293–301. doi: 10.1159/000381727

Liebeskind, D. S. (2005). Collaterals in acute stroke: beyond the clot. *Neuroimaging Clin. N. Am.* 15, 553–73, x. doi: 10.1016/j.nic.2005.08.012

Lima, F. O., Furie, K. L., Silva, G. S., Lev, M. H., Camargo, E. C., Singhal, A. B., et al. (2014). Prognosis of untreated strokes due to anterior circulation proximal intracranial arterial occlusions detected by use of computed tomography angiography. *JAMA Neurol.* 71, 151–157. doi: 10.1001/jamaneurol.2013.5007

Liu, Y., Chen, Y. T., Zhang, C., and Zhou, P. (2022). Motor unit distribution and recruitment in spastic and non-spastic bilateral biceps brachii muscles of chronic stroke survivors. *J. Neural Eng.* 19:046047. doi: 10.1088/1741-2552/ac86f4

Liu, X., Zhou, M., Zhao, J., Gao, Y., Wang, Y., Zhou, J., et al. (2022). Functional Independence and disability evaluation in stroke patients: optimal cutoff scores for a pictorial-based Longshi scale, Barthel index, and modified Rankin scale. *Front. Neurol.* 13:710852. doi: 10.3389/fneur.2022.710852

Malik, N., Hou, Q., Vagal, A., Patrie, J., Xin, W., Michel, P., et al. (2014). Demographic and clinical predictors of leptomeningeal collaterals in stroke patients. *J. Stroke Cerebrovasc. Dis.* 23, 2018–2022. doi: 10.1016/j.jstrokecerebrovasdis.2014.02.018

Moffat, B. A., Chenevert, T. L., Lawrence, T. S., Meyer, C. R., Johnson, T. D., Dong, Q., et al. (2005). Functional diffusion map: a non-invasive MRI biomarker for early stratification of clinical brain tumor response. *Proc. Natl. Acad. Sci. U. S. A.* 102, 5524–5529. doi: 10.1073/pnas.0501532102

Mouridsen, K., Friston, K., Hjort, N., Gyldensted, L., Ostergaard, L., and Kiebel, S. (2006). Bayesian estimation of cerebral perfusion using a physiological model of microvasculature. *NeuroImage* 33, 570–579. doi: 10.1016/j.neuroimage.2006.06.015

Olivot, J. M., Mlynash, M., Thijs, V. N., Kemp, S., Lansberg, M. G., Wechsler, L., et al. (2009a). Optimal Tmax threshold for predicting penumbral tissue in acute stroke. *Stroke* 40, 469–475. doi: 10.1161/STROKEAHA.108.526954

Olivot, J. M., Mlynash, M., Zaharchuk, G., Straka, M., Bammer, R., Schwartz, N., et al. (2009b). Perfusion MRI (Tmax and MTT) correlation with xenon CT cerebral blood flow in stroke patients. *Neurology* 72, 1140–1145. doi: 10.1212/01.wnl.0000345372.49233.e3

Ong, E., Eker, O., Chamard, L., Cho, T. H., Derex, L., Buisson, M., et al. (2019). MRI profile and collateral status in patients with a transient ischemic attack and an intracranial artery occlusion. *J. Neuroimaging* 29, 187–189. doi: 10.1111/jon.12560

Ostergaard, L. (2005). Principles of cerebral perfusion imaging by bolus tracking. *J. Magn. Reson. Imaging* 22, 710–717. doi: 10.1002/jmri.20460

Park, H. I., Cha, J. K., Kang, M. J., Kim, D. H., Yoo, N. T., Choi, J. H., et al. (2011). Reduced rCBV ratio in perfusion-weighted MR images predicts poor outcome after thrombolysis in acute ischemic stroke. *Eur. Neurol.* 65, 257–263. doi: 10.1159/000324727

Park, H. S., Cha, J. K., Kim, D. H., Kang, M. J., Choi, J. H., and Huh, J. T. (2014). The rCBV ratio on perfusion-weighted imaging reveals the extent of blood flow on conventional angiography after acute ischemic stroke. *Clin. Neurol. Neurosurg.* 122, 54–58. doi: 10.1016/j.clineuro.2014.04.001

Provost, C., Soudant, M., Legrand, L., Ben Hassen, W., Xie, Y., Soize, S., et al. (2019). Magnetic resonance imaging or computed tomography before treatment in acute ischemic stroke. *Stroke* 50, 659–664. doi: 10.1161/strokeaha.118.023882

Richardson, J. D., Baker, J. M., Morgan, P. S., Rorden, C., Bonilha, L., and Fridriksson, J. (2011). Cerebral perfusion in chronic stroke: implications for lesion-symptom mapping and functional MRI. *Behav. Neurol.* 24, 117–122. doi: 10.3233/ben-2011-0283

Rost, N. S., and Brodtmann, A. (2022). Post-stroke cognitive impairment and dementia. *Circ. Res.* 130, 1252–1271. doi: 10.1161/circresaha.122.319951

Schmidt, M. A., Engelhorn, T., Lang, S., Luecking, H., Hoelter, P., Fröhlich, K., et al. (2020). DSC brain perfusion using advanced deconvolution models in the diagnostic work-up of dementia and mild cognitive impairment: a Semiquantitative comparison with HMPAO-SPECT-brain perfusion. *J. Clin. Med.* 9:1800. doi: 10.3390/jcm9061800

Sennfält, S., Pihlsgård, M., Norrving, B., and Ullberg, T. (2021). Ischemic stroke patients with prestroke dependency: characteristics and long-term prognosis. *Acta Neurol. Scand.* 143, 78–88. doi: 10.1111/ane.13328

Shih, L. C., Saver, J. L., Alger, J. R., Starkman, S., Leary, M. C., Vinuela, F., et al. (2003). Perfusion-weighted magnetic resonance imaging thresholds identifying core, irreversibly infarcted tissue. *Stroke* 34, 1425–1430. doi: 10.1161/01.str.0000072998.70087.e9

Singer, O. C., de Rochemont Rdu, M., Foerch, C., Stengel, A., Lanfermann, H., Sitzer, M., et al. (2003). Relation between relative cerebral blood flow, relative cerebral blood volume, and mean transit time in patients with acute ischemic stroke determined by perfusion-weighted MRI. *J. Cereb. Blood Flow Metab.* 23, 605–611. doi: 10.1097/01.wcb.0000062342.57257.28

Sohn, S. W., Park, H. S., Cha, J. K., Kim, D. H., Kang, M. J., Choi, J. H., et al. (2016). Relative CBV ratio on perfusion-weighted MRI indicates the probability of early recanalization after IV t-PA administration for acute ischemic stroke. *J. Neurointerv. Surg.* 8, 235–239. doi: 10.1136/neurintsurg-2014-011501

Thompson, J. W., Dave, K. R., Young, J. I., and Perez-Pinzon, M. A. (2013). Ischemic preconditioning alters the epigenetic profile of the brain from ischemic intolerance to ischemic tolerance. *Neurotherapeutics* 10, 789–797. doi: 10.1007/s13311-013-0202-9

Tian, G., Ji, Z., Lin, Z., Pan, S., and Yin, J. (2021). Cerebral autoregulation is heterogeneous in different stroke mechanism of ischemic stroke caused by intracranial atherosclerotic stenosis. *Brain Behav.* 11:e01907. doi: 10.1002/brb3.1907

Tsai, Y. H., Hsu, L. M., Weng, H. H., Lee, M. H., Yang, J. T., and Lin, C. P. (2013). Functional diffusion map as an imaging predictor of functional outcome in patients with primary intracerebral haemorrhage. *Br. J. Radiol.* 86:20110644. doi: 10.1259/bjr.20110644

Tsien, C., Galbán, C. J., Chenevert, T. L., Johnson, T. D., Hamstra, D. A., Sundgren, P. C., et al. (2010). Parametric response map as an imaging biomarker to distinguish progression from pseudoprogression in high-grade glioma. *J. Clin. Oncol.* 28, 2293–2299. doi: 10.1200/jco.2009.25.3971

Vilela, P., and Rowley, H. A. (2017). Brain ischemia: CT and MRI techniques in acute ischemic stroke. *Eur. J. Radiol.* 96, 162–172. doi: 10.1016/j.ejrad.2017.08.014

Wang, H., Lin, J., Zheng, L., Zhao, J., Song, B., and Dai, Y. (2020). Texture analysis based on ADC maps and T2-FLAIR images for the assessment of the severity and prognosis of ischaemic stroke. *Clin. Imaging* 67, 152–159. doi: 10.1016/j.clinimag.2020.06.013

Whiteley, W. N., and Gupta, A. K. (2021). Long-term incidence of stroke and dementia in ASCOT. *Stroke* 52, 3088–3096. doi: 10.1161/strokeaha.120.033489

Winship, I. R. (2015). Cerebral collaterals and collateral therapeutics for acute ischemic stroke. *Microcirculation* 22, 228–236. doi: 10.1111/micc.12177

Włodarczyk, L., and Cichon, N. (2022). Neuroimaging techniques as potential tools for assessment of angiogenesis and neuroplasticity processes after stroke and their clinical implications for rehabilitation and stroke recovery prognosis. *J. Clin. Med.* 11:2473. doi: 10.3390/jcm11092473

Yao, B., Klein, C. S., Hu, H., Li, S., and Zhou, P. (2018). Motor unit properties of the first dorsal interosseous in chronic stroke subjects: concentric needle and single Fiber EMG analysis. *Front. Physiol.* 9:1587. doi: 10.3389/fphys.2018.01587